Journal of Quantitative Spectroscopy & Radiative Transfer 111 (2010) 2534–2549

Contents lists available at ScienceDirect

Journal of Quantitative Spectroscopy & Radiative Transfer

journal homepage: www.elsevier.com/locate/jqsrt

The impact of ice particle roughness on the scattering phase matrix

Bryan A. Baum [a,*], Ping Yang [b], Yong-Xiang Hu [c], Qian Feng [b]

[a] Space Science and Engineering Center, University of Wisconsin-Madison, 1225 W. Dayton Street, Madison, WI 53706, USA
[b] Texas A&M University, College Station, TX, USA
[c] NASA Langley Research Center, Hampton, VA, USA

ARTICLE INFO

Article history:
Received 15 March 2010
Received in revised form
16 July 2010
Accepted 19 July 2010

Keywords:
Ice crystals
Polarized reflectance
Scattering
Radiative transfer
Clouds

ABSTRACT

The goal of this study is to explore the influence of ice particle habit (or shape) and surface roughness on the scattering phase matrix. As an example, reported here are the results for two wavelengths: 0.67 and 1.61 μm. For this effort, a database of single-scattering properties has been computed for a set of habits including hexagonal plates, hollow and solid columns, hollow and solid 3D bullet rosettes, droxtals, aggregates of solid columns, and aggregates of plates. The database provides properties for each of the habits at 101 wavelengths between 0.45 and 2.24 μm for smooth, moderately roughened, and severely roughened particles. At each wavelength, the scattering properties are provided at 233 discrete particle diameters ranging from 2 to 10,000 μm. A single particle size distribution from a very cold ice cloud sampled during the CRYSTAL-FACE field campaign (T_{cld}=−76 °C) is used to illustrate the influence of habit and roughness on the phase matrix. In all, four different habit mixtures are evaluated. The nonzero elements of the phase matrix are shown to be quite sensitive to the assumed habit, particularly in the case of $-P_{12}/P_{11}$ that is associated with the degree of linear polarization of scattered radiation. Surface roughness is shown to smooth out maxima in the scattering phase function and in the other elements of the phase matrix, consistent with other studies. To compare with the theoretical simulations of the phase matrix for smooth and roughened particles, a full year of cloud-aerosol lidar with orthogonal polarization (CALIOP) data from 2008 is analyzed to provide global statistics on the values of P_{11} and P_{22}/P_{11} in the backscattering direction. In a comparison of two of the habit mixtures (one used for MODIS Collection 5 and another that incorporates new habits including hollow bullet rosettes and aggregates of plates) with the CALIOP data, the values for P_{11} are higher regardless of the degree of particle surface roughness, and the values for P_{22}/P_{11} are lower than those for CALIOP. Further investigation is warranted to better understand this discrepancy.

1. Introduction

The wealth of data available from both the A-Train and geostationary satellite platforms provides a unique opportunity to perform detailed analyses of ice clouds using both active and passive remote sensing techniques. For studies of ice clouds based on the moderate resolution imaging spectroradiometer (MODIS), particular attention has been focused on the development of the bulk scattering and absorption models that are used to build static look-up tables (LUTs) of reflection/transmission characteristics [1,2]. These LUTs are essential to the global retrievals of cloud optical thickness and effective particle size. The radiative characteristics of ice clouds also have a dependence on the ice habits [3]. Solar spectral observations have been used in a variety of studies to determine cloud properties [4,5]. Differences in global cloud products obtained with the updated scattering models

* Corresponding author. Tel.: +1 608 263 3898; fax: +1 608 262 5974.
E-mail address: bryan.baum@ssec.wisc.edu (B.A. Baum).

0022-4073/$ - see front matter © 2010 Elsevier Ltd. All rights reserved.
doi:10.1016/j.jqsrt.2010.07.008

between collections 4 and 5 are detailed in Yang et al. [6]. However, the ice particles used to date have smooth facets that have strong angular features in the scattering phase functions at visible and shortwave infrared (SWIR) wavelengths (e.g., maxima at forward scattering angles of 22° and 46° as well as in the backscattering at 156° and 180°). Zhang et al. [7] show that a seasonal component can be introduced into the products if the assumed scattering phase function has pronounced angular features such as those produced with smooth particles.

The question we are beginning to address, based on our evaluation of the MODIS ice cloud products, concerns a fundamental property of the ice habits used to develop the LUTs involved in the operational retrievals: whether to assume the ice particles have smooth or roughened facets. The occurrence of halos and sundogs in cirrus suggests the presence of some relatively smooth faceted particles. In the geometric optics limit, the polarization state of a reflected ray depends on the incidence angle and reaches 100% at the Brewster angle [8], at which there is no reflection for the electric field component parallel to the incident plane. Particles with rough surfaces tend to depolarize the radiation beam because the random orientations of the small facets on the roughened surface reduce the chance for rays to undergo polarized reflection associated with the Brewster angle.

Both theoretical and laboratory studies of ice particles [9–12] show the influence of roughening on polarization properties. The assumption of surface roughness also influences the interpretation of lidar depolarization measurements, since the lidar backscatter decreases with increasing roughness. The roughness also impacts an assumption of the amount of forward scattering in a lidar beam, which is necessary for determining the extinction in the column being measured. In a larger context, the assumption of whether ice particles should be smooth or roughened actually has implications for understanding of global ice cloud properties and their influence on the radiation budget, and can impact cloud climatologies in subtle ways that we are only now beginning to appreciate.

If it is determined that roughened particles are more appropriate for global cloud retrieval efforts, how much roughening should be applied in the scattering calculations for individual particles? The key to understanding how to better incorporate some amount of ice particle roughness in the LUTs may be provided by the measurements of the polarization of single scattering events. The polarization and directionality of the Earth reflectance (POLDER) instrument, which has flown on ADEOS-1/-2 and PARASOL, has polarization capability in three visible/shortwave-infrared (VIS/SWIR) spectral channels at up to 14 viewing angles, with resulting scattering angles between 60° and 180° (depending on region and time of year). The POLDER observations contain a wealth of information about cloud properties [13–16]. A global aggregation of ice cloud polarization as a function of scattering angle suggested that a relatively smooth phase function is consistent with global observations [17]. Zhang et al. [7] investigated the impact of the phase function on the global derivation of ice cloud optical thickness in a study based on MODIS and POLDER analyses. As expected, optical thickness retrievals can differ substantially depending on the assumed ice scattering phase functions. The optical thicknesses inferred from POLDER were lower than those obtained from MODIS. Further investigation suggested that this difference could be caused by the assumption of an inhomogeneous ice model (IHM; [17]) for POLDER that has a lower value of the asymmetry parameter g than that obtained from the smooth ice particle models used by MODIS.

Section 2 provides information and background on the data and models. Section 3 provides the phase matrix properties obtained from integration over a given particle size and habit distribution. Section 4 provides analysis of a full year of data (2008) from the cloud-aerosol lidar with orthogonal polarization (CALIOP) on the cloud-aerosol lidar and infrared pathfinder satellite observation (CALIPSO) satellite platform. The study is summarized in Section 5.

2. Data and models

2.1. Single-scattering properties

Previous calculations of the single-scattering properties for individual ice particles have been reported for hollow and solid columns, hexagonal plates, 3D solid bullet rosettes, and aggregates of solid columns [18,19]. Recently, a bullet rosette with hollow structures was developed [20]. Bi et al. [21] summarize a number of improvements that have become available for light scattering calculations with regards to the use of the improved geometric optics method (IGOM). The Collection 5 MODIS models [2] contained a delta-transmission term that accounted for the energy associated with rays that pass through two opposing (flat) facets of a hexagonal ice particle without scattering. However, this is an artifact of the treatment of forward scattering in the numerical implementation of the IGOM. A new treatment of ray spreading has been incorporated for forward scattering that now obviates the delta-transmission term [21]. Other improvements to the scattering calculations now result in more consistent efficiency factors from small to large size parameters ($\kappa=2\pi r/\lambda$, where r is radius and λ is wavelength) and more detail in the scattering phase function at backscattering angles. The discretization of the particle size has been increased with the new simulations. Yang et al. [22] discuss the treatment of surface roughness for light scattering calculations involving solid columns. Basically, surface roughness is treated by assuming that a particle surface is composed of small facets that can be randomly tilted, and subsequently sampled for different realizations whereupon the amount of tilt follows a Gaussian distribution. The root-mean-square tilt σ is given by $\sigma=0$ for smooth particles, $\sigma=0.03$ for moderately roughened particles and $\sigma=0.5$ for severely roughened particles. Finally, the new single-scattering property computations are based on the ice refractive index reported by Warren and Brandt [23].

For the computations reported in this study, a database of single-scattering properties was prepared for droxtals, hollow and solid columns, hollow and solid bullet rosettes, and aggregates of columns. Additionally, two new habits are included for the first time, consisting of a "small" aggregate of plates consisting of five plates, and a "large" aggregate of plates that have more plates in the particle. The guidance being followed is that no individual plate can grow to more than 500 μm in an aggregate. The small aggregate of plates is used for particles having $D_{\max} \leq 1250$ μm, while the large aggregate of plates is used for particles having $D_{\max} \geq 800$ μm.

2.2. Mueller matrix

The development of an algorithm for retrieving ice cloud properties from polarimetric measurements requires a polarized (or vector) radiative transfer (RT) model [24] that accounts for the Stokes parameters. In principle, the Stokes parameters observed by a sensor can be expressed as follows:

$$\begin{bmatrix} I_s \\ Q_s \\ U_s \\ V_s \end{bmatrix} = \begin{bmatrix} M_{11} & M_{12} & M_{13} & M_{14} \\ M_{21} & M_{22} & M_{23} & M_{24} \\ M_{31} & M_{32} & M_{33} & M_{34} \\ M_{41} & M_{42} & M_{43} & M_{44} \end{bmatrix} \begin{bmatrix} I_i \\ Q_i \\ U_i \\ V_i \end{bmatrix}, \quad (1)$$

where (I_i, Q_i, U_i, V_i) and (I_s, Q_s, U_s, V_s) are the incident and scattered Stokes parameters, respectively. The matrix $[M_{i,j}]$ is called the effective Mueller matrix [25]. In the case of radiative transfer involving ice clouds, the effective Mueller matrix contains a wealth of information for retrieving ice cloud properties. The sensitivity of the Mueller matrix to particle shape has been studied [26], but the influence of particle roughening on the Mueller matrix has not been adequately explored.

An imager such as MODIS provides only the intensity of the radiation field (M_{11}) from a field of scattering particles. As demonstrated by Kattawar and Rakovic [25], the phase matrix element M_{11} is the least sensitive to small changes in particle morphology (i.e., particle size and shape) and dielectric properties (i.e., the refractive index). The shortcoming of a retrieval approach based on the intensity component alone was discussed for the case of aerosols [27].

Natural sunlight is unpolarized, that is, $(I_i, Q_i, U_i, V_i)=(I_i, 0, 0, 0)$. Polarimetric sensors such as POLDER observe intensity and linear polarization, i.e., the first three Stokes parameters (I, Q and U). For such a sensor, it is apparent from Eq. (1) that only the M_{11}, M_{21} and M_{31} elements of the effective Mueller matrix can be obtained from the Stokes parameters. More insight into ice particle roughening may be gained by fully understanding the information contained in the M_{21} and M_{31} elements in addition to the information content in M_{11}.

2.3. CALIOP data

On the cloud-aerosol lidar and infrared pathfinder satellite observation (CALIPSO) satellite platform, there is a nadir-viewing lidar called the cloud-aerosol lidar with orthogonal polarization (CALIOP). CALIOP takes data at 532 and 1064 nm, and the former channel provides information on both the P_{11} and P_{22}/P_{11} components of the phase matrix. CALIPSO flies information with NASA's Earth Observation System Aqua platform and is part of the A-Train suite of sensors.

3. Phase matrix obtained from integration over particle size and habit distribution

In this section, the phase matrix is calculated at two wavelengths, 0.67 and 1.61 μm, by integrating the individual ice habit scattering properties over a single particle size distribution (PSD) but for four different assumed habit distributions. The three habit distributions are for (1) a combination of droxtals (for only the smallest particles in a given PSD) and solid columns, (2) a mixture of droxtals (small particles only) and hollow bullet rosettes, (3) the habit mixture used for MODIS collection 5 ice clouds, and (4) a new habit mixture under development that incorporates the new particle habits.

The MODIS Collection 5 (henceforth C5) habit distribution is as follows: $D_{\max} \leq 60$ μm, 100% droxtals; $60 < D_{\max} \leq 1000$ μm, 15% 3D bullet rosettes, 50% solid columns, 35% plates; $1000 < D_{\max} \leq 2000$ μm, 45% hollow columns, 45% solid columns, 10% aggregates; and $D_{\max} > 2000$ μm, 97% 3D bullet rosettes, 3% aggregates. Neither the hollow bullet rosette particle nor the aggregate of plates particle was available at the time this habit distribution was derived. However, a new habit distribution, shown in Fig. 1, is under development that includes three new habits: hollow bullet rosettes, and a "small" and "large" aggregate of plates. The "small" aggregate of plates is composed of five individual plates and is used to represent particles having a maximum dimension of less than about 1200 μm in maximum dimension. The "large" aggregate of plates is composed of more individual plates, and is used to represent particles from 800 to 10,000 μm in maximum dimension. With the new habit distribution, the percentages of each ice habit vary smoothly with size rather than having discontinuous jumps as with the C5 distribution.

The PSD is described by a gamma distribution [28] of the form:

$$n(D_{\max}) = N_0 D_{\max}^{\mu} e^{-\lambda D_{\max}} \quad (2)$$

where $D_{\max}$ is the particle maximum dimension, $n(D)$ is the particle concentration per unit volume, N_0 is the intercept, λ is the slope, and μ is the dispersion. Fig. 2 shows the PSD chosen for illustrative purposes. This particular PSD is from extremely cold cirrus ($T_{\text{cld}} = -76$ °C) sampled during the CRYSTAL-FACE field campaign and has gamma coefficients as follows: $N_0 = 0.44$, $\lambda = 3667\ \text{cm}^{-1}$, and $\mu = -0.57$.

The effective diameter D_{eff} is defined as

$$D_{eff} = \frac{3}{2} \frac{\sum_{h=1}^{M} \left[\int_{D\min}^{D\max} V_h(D) n(h,D) f_h(D) dD \right]}{\sum_{h=1}^{M} \left[\int_{D\min}^{D\max} A_h(D) n(h,D) f_h(D) dD \right]}, \quad (3)$$

where $V_h(D)$ is the volume of the particle for habit h, $A_h(D)$ is the projected area of an ice particle for a given habit, $f_h(D)$ is the ice particle habit fraction for habit h, M is the number of habits, D is particle size, and $n(D)$ is the particle

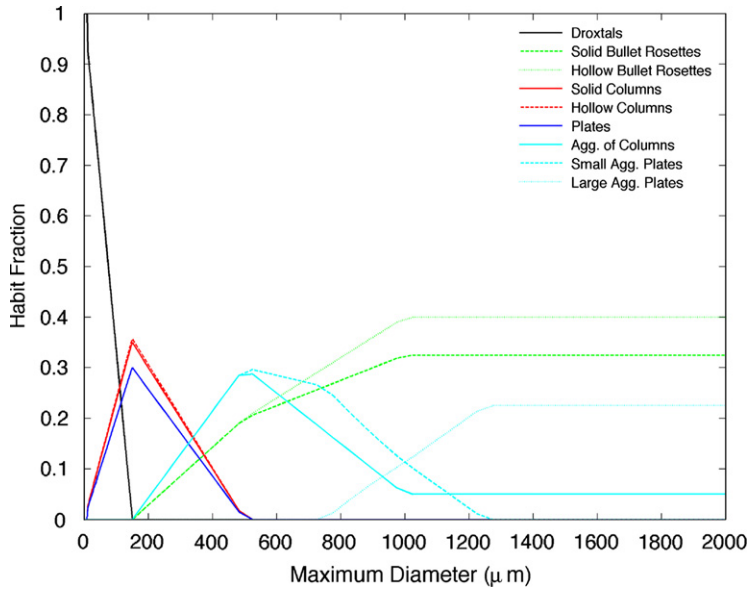

Fig. 1. New habit distribution developed to include new habits such as the hollow bullet rosette and aggregate of plates.

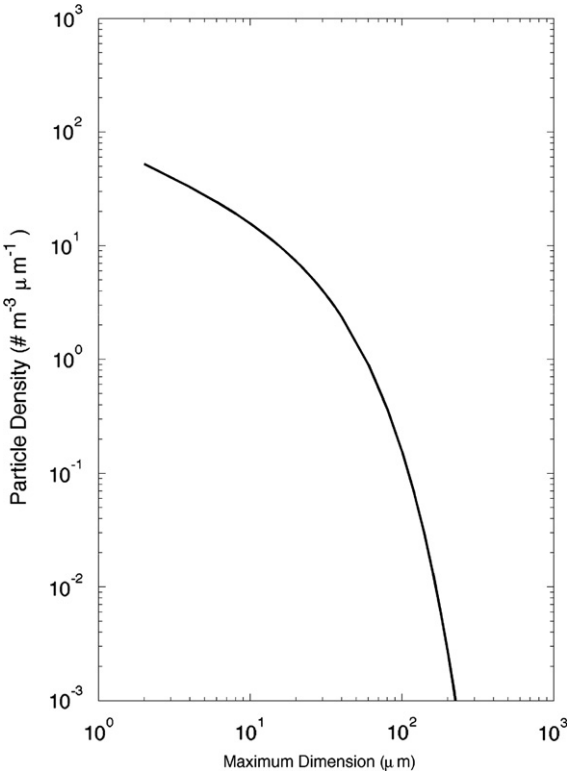

Fig. 2. Particle size distribution from cirrus at $T_{cld}=-76\,^{\circ}C$ during the CRYSTAL-FACE field campaign.

density. The habit fraction is defined so that for each size bin,

$$\sum_{h=1}^{M} f_h(D) = 1. \tag{4}$$

The phase matrix obtained by integrating over a PSD at a given wavelength is given by

$$\overline{P_{ij}}(\Theta) = \frac{\int_{D\min}^{D\max}\left[\sum_{h=1}^{M} P_{ij,h}(\Theta,D)\sigma_{sca,h}(D)f_h(D)\right]n(D)dD}{\int_{D\min}^{D\max}\left[\sum_{h=1}^{M}\sigma_{sca,h}(D)f_h(D)\right]n(D)dD}, \tag{5}$$

where $P_{ij,\ h}(D)$ is the phase matrix component and $\sigma_{sca,\ h}(D)$ is the scattering cross section for each of the ice particle habits.

For the PSD in Fig. 2, results are provided in Figs. 3 (λ=0.67 μm) and 4 (λ=1.61 μm) for a habit mixture defined as a combination of droxtals for ice particles having $D_{max} \leq 20$ μm and solid columns for larger particles. For this PSD and habit mixture, the D_{eff} is 43 μm. We note that solid columns have a higher volume per particle than either solid bullet rosettes or hollow columns, so use of solid columns will result in higher values of D_{eff} than for habit mixtures that use less dense particles. Each panel in these figures shows results based on a mixture of smooth particles (solid line), moderately roughened particles (dashed line), or severely roughened particles (dotted line). Fig. 3 shows that for smooth particles in the P_{11} component, maxima are found at forward scattering angles, such as the peak at Θ=22°, as well as at backscattering angles, such as at Θ=150° and 180°. The asymmetry parameter at λ=0.67 μm for smooth, moderately roughened, and severely roughened particles is 0.7889, 0. 7850, and 0.7724, respectively. The difference between smooth and moderately roughened particles is not large, and this may be due in part to the use of a PSD from a very cold cloud so that there are no particles larger than about 200 μm. However, the asymmetry parameter is reduced more for severely roughened particles.

The $(-P_{12}/P_{11})$ component is known as the degree of linear polarization of natural (i.e., non-polarized) incident light [29]. Inspection of this component in Figs. 3 and 4 indicates that the degree of linear polarization can have both

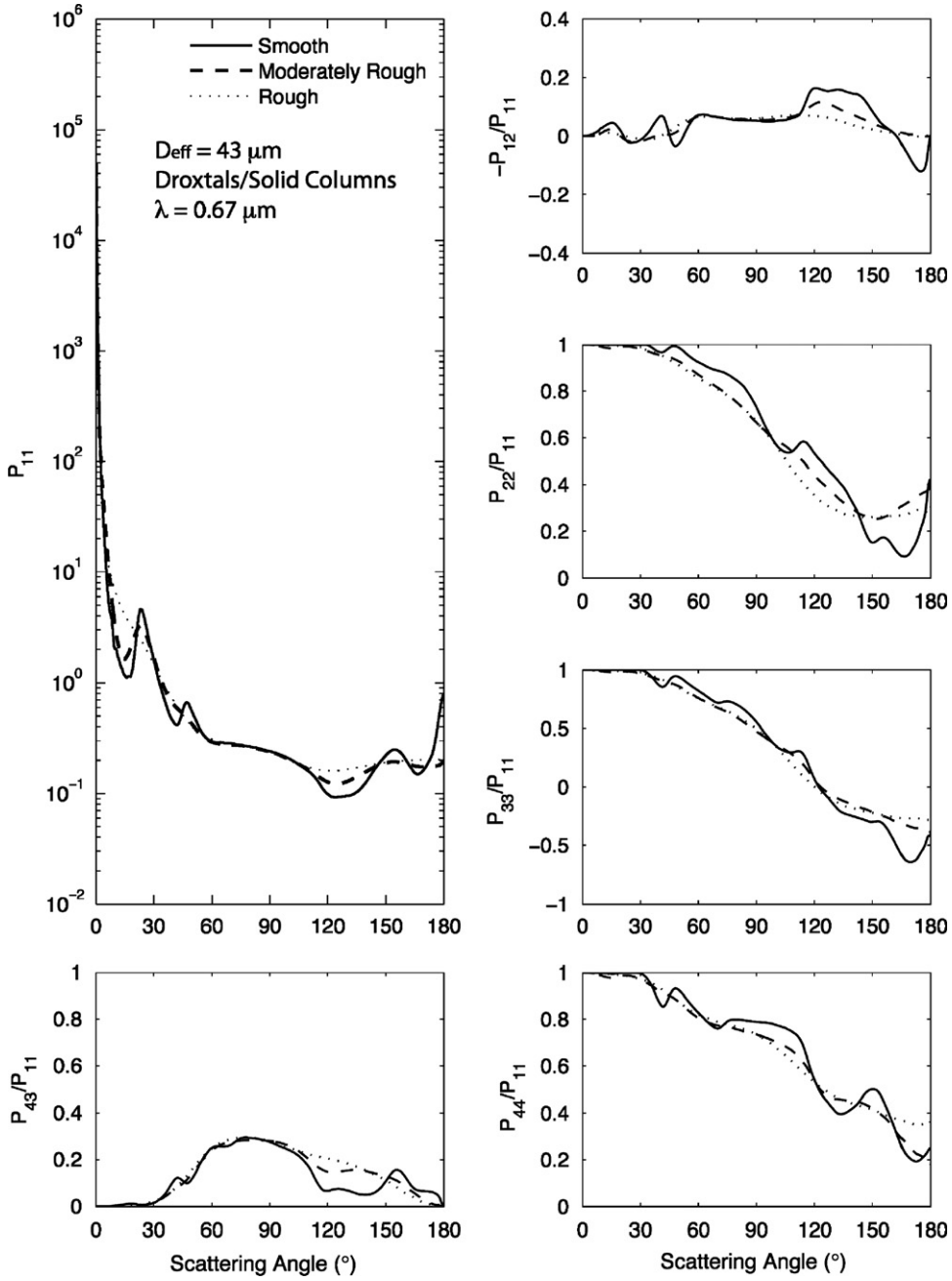

Fig. 3. Phase matrix for the PSD in Fig. 2, but assuming droxtals for the smallest particles ($D_{max} < 20$ μm) and solid columns for larger particles. The wavelength is 0.67 μm and the D_{eff} is 43 μm. The values of the asymmetry parameter for smooth, moderately roughened, and severely roughened particles are 0.7889, 0. 7850, and 0.7724, respectively.

positive and negative values. External reflections result in positive polarization values whereas internal reflections have negative values. The inclusion of surface roughening tends to smooth out the peaks, leading to smoother phase matrix components. In both Figs. 3 and 4, it is interesting to note that between $\Theta = 120^\circ$ and 140°, there is an increase in the degree of linear polarization for smooth particles, which is an indication of an increase in external reflection.

The P_{22}/P_{11} component is also of interest in this study because measurements are available at $\Theta = 180^\circ$ by CALIOP, and is discussed further in Section 4. For spherical particles, $P_{11} = P_{22}$ so that $P_{22}/P_{11} = 1$. The term P_{22}/P_{11} will depart from a value of 1 as the nonsphericity of the particles increases, and is thus referred to as an indicator of "particle nonsphericity" [29]. Inspection of Figs. 3 and 4 for this component shows that the value of P_{22}/P_{11} has some sensitivity to particle roughening at the backscattering angle. While the difference in the value of P_{22}/P_{11} is not large for smooth versus moderately roughened particles, the difference between

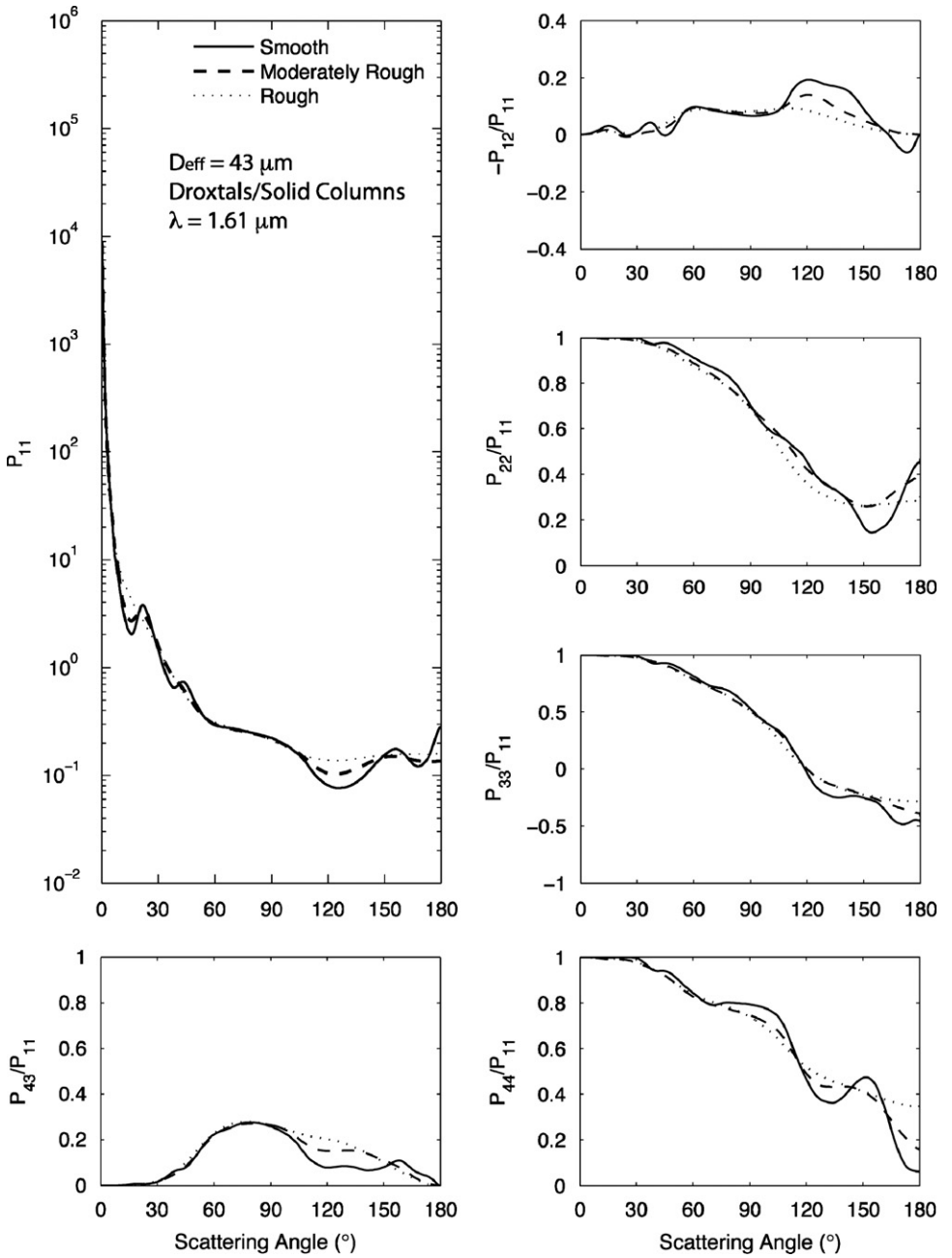

Fig. 4. Same as for Fig. 3 but at a wavelength of 1.61 μm. The values of the asymmetry parameter for smooth, moderately roughened, and severely roughened particles are 0.8147, 0.8069, and 0.7951, respectively.

smooth and severely roughened particles is more pronounced.

Figs. 5 (λ=0.67 μm) and 6 (λ=1.61 μm) show results based on the use of a combination of droxtals for ice particles ($D_{\max} \leq 20$ μm) and hollow bullet rosettes for larger particles. The D_{eff} for this habit distribution is only 16 μm and is much lower than that for solid columns because hollow bullet rosettes have a much lower volume as a function of particle size than solid columns. For smooth particles, Fig. 5 indicates the presence of two halos in the P_{11} component at forward scattering angles (Θ=10° and 22°) but not at Θ=46°. It is also interesting to note that there is no enhancement in the side or backscattering directions, i.e., at Θ=150° or 180°. These figures indicate that particle habit can exert a strong influence on the amount of backscattering, with features that show up in the degree of linear polarization. In Fig. 6, there is only one halo apparent in the P_{11} component at Θ=22°; the rest of the phase function is fairly smooth. Again, particle roughening smooths out the features in the various phase matrix components. The values of the asymmetry parameter at λ=0.67 μm for

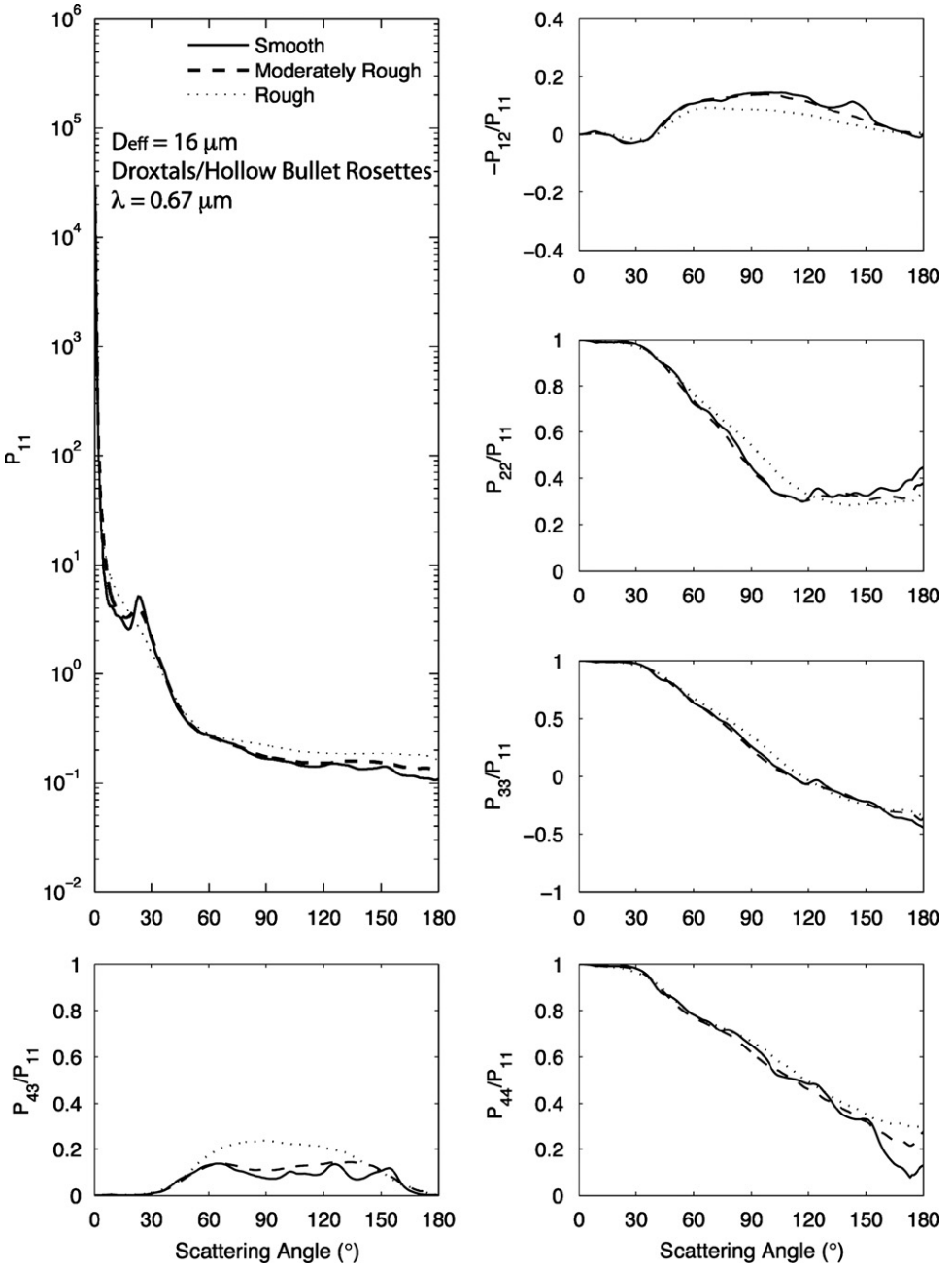

Fig. 5. Phase matrix for the PSD in Fig. 2, but assuming droxtals for the smallest particles ($D_{max} < 20$ μm) and hollow bullet rosettes for larger particles. The wavelength is 0.67 μm and the D_{eff} is 16 μm. The values of the asymmetry parameter for smooth, moderately roughened, and severely roughened particles are 0.7992, 0.8000, and 0.7703, respectively.

smooth, moderately roughened, and severely roughened particles are 0.7992, 0.8000, and 0.7703, respectively. As with the previous case assuming solid columns, the asymmetry parameter for smooth and moderately roughened particles is quite similar, but is noticeably lower when the particles are severely roughened.

Fig. 7 shows the phase matrix computed at a wavelength of 0.67 μm for the chosen PSD using the MODIS Collection 5 habit distribution [1]. The C5 habit distribution does not include either hollow bullet rosettes or small/large aggregates of plates. The D_{eff} for this habit distribution is 40 μm. In the P_{11} component for smooth particles, there are several maxima notable at forward scattering angles ($\Theta = 10^{\circ}$, 22°, and 46°), as well as at approximately $\Theta = 150^{\circ}$ and at backscattering ($\Theta = 180^{\circ}$). The enhancement at backscattering seems to be a result of the use of such a high percentage of pristine particles such as solid columns and plates. The asymmetry parameter at $\lambda = 0.67$ μm for smooth, moderately roughened, and severely roughened particles is 0.8078, 0.8003, and 0.7630, respectively.

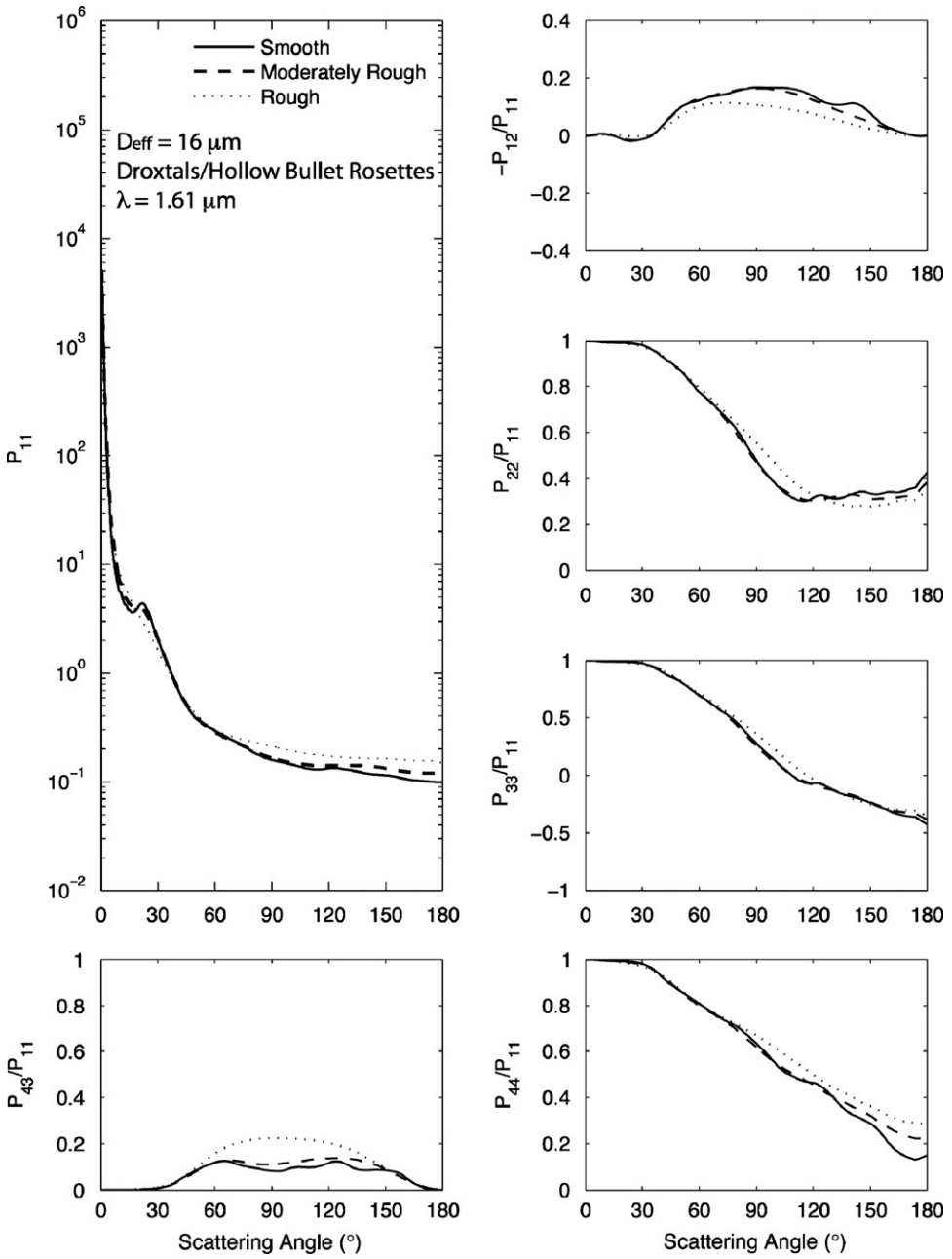

Fig. 6. Same as for Fig. 5 but at a wavelength of 1.61 μm. The values of the asymmetry parameter for smooth, moderately roughened, and severely roughened particles are 0.8103, 0.8097, and 0.7807, respectively.

Fig. 8 shows similar results but at a wavelength of 1.61 μm. The absorption within the various ice particles is higher at this wavelength and this acts to reduce the magnitude of the maxima in the P_{11} component at $\Theta=22^\circ$, and 46°; the halo at $\Theta=10^\circ$ is no longer apparent. For both Figs. 7 and 8, the P_{22}/P_{11} component at backscattering indicates that there are differences between smooth, moderately roughened, and severely roughened particles.

Figs. 9 ($\lambda=0.67$ μm) and 10 ($\lambda=1.61$ μm) show the phase matrix computed for the chosen PSD using the new habit distribution (Fig. 1b). Compared to the results in Figs. 7 and 8 for the C5 habit distribution, these results display some interesting differences. Most notably, the inclusion of the hollow bullet rosette particle has dampened the backscattering component ($\Theta=180^\circ$) of the P_{11} component. The values of the asymmetry parameter at $\lambda=0.67$ μm for smooth, moderately roughened, and severely roughened particles are 0.8078, 0.8003, and 0.7630, respectively, which are quite similar to those determined using the C5 habit mixture. As with our previous results, there are differences between smooth, moderately roughened, and severely roughened particles in the P_{22}/P_{11}

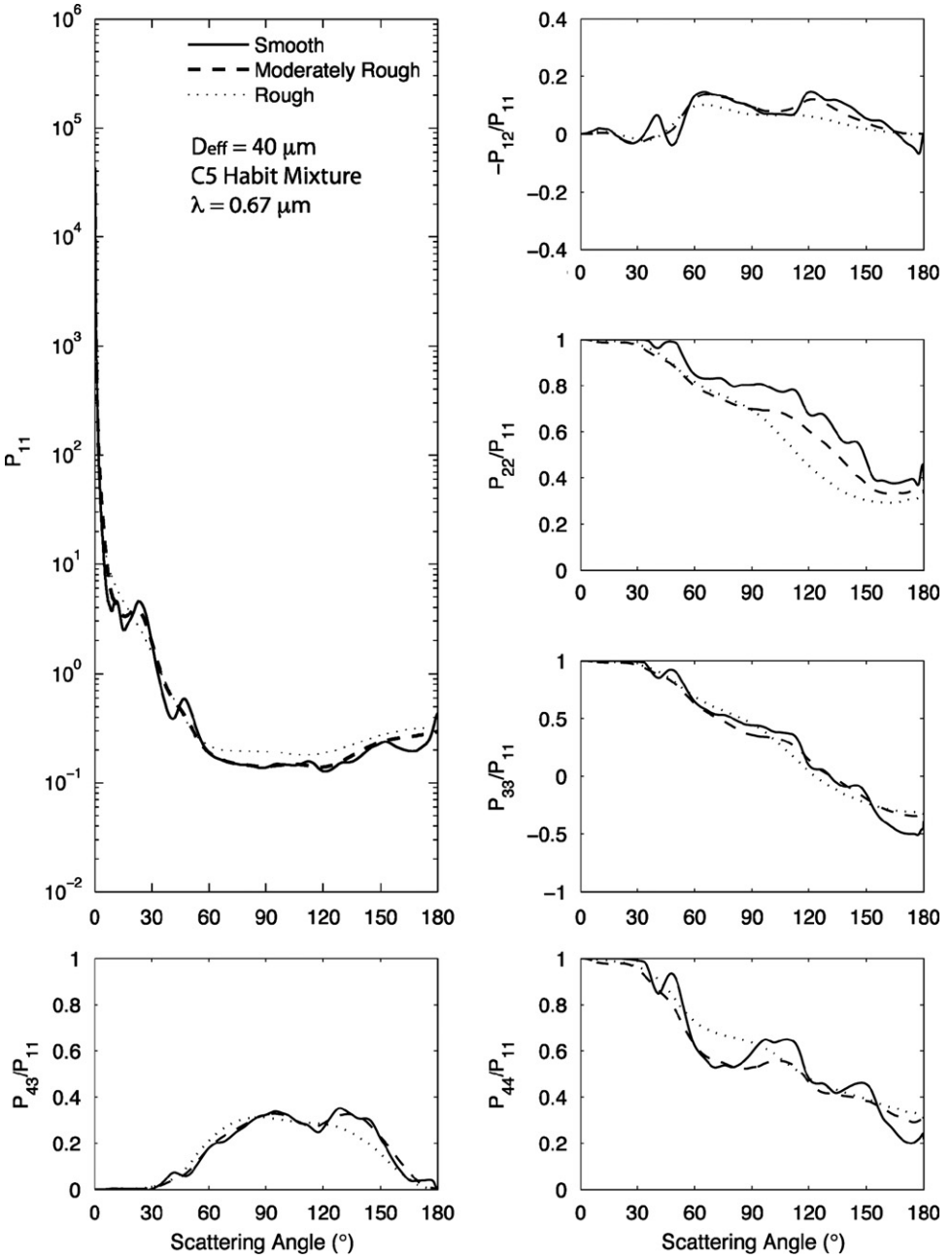

Fig. 7. Phase matrix for the PSD in Fig. 2, using the MODIS Collection 5 (C5) habit distribution. The wavelength is 0.67 μm and the D_{eff} is 40 μm. The values of the asymmetry parameter for smooth, moderately roughened, and severely roughened particles are 0.8077, 0.7999, and 0.7613, respectively.

component at $\Theta = 180^{\circ}$ regardless of the habit mixture used, indicating that there is sensitivity to both habit and roughness at this angle. This is significant since it provides an opportunity to gain further insight through comparison with depolarization lidar measurements.

Fig. 11 shows a polar plot of the individual Mueller matrix components for smooth and roughened ice particles for the PSD shown in Fig. 2, for an assumed habit distribution given by MODIS Collection 5, a wavelength of 0.67 μm, a solar zenith angle of 24°, and an ice cloud optical thickness of 1. For these polar plots, the radius from the center denotes the view zenith angle (nadir in the center, increasing to 90° at the outer boundary of the polar plot), while the relative azimuth angle rotates through 360°, with 0° as the forward scattering angle. What is immediately evident is that the elements of the Mueller matrix are sensitive to the roughness of the ice particles, including the M_{21}/M_{11} component. Based on these calculations, space-based polarization measurements will be very useful for determining how much roughness naturally occurring ice particles have in different climatic regimes and under

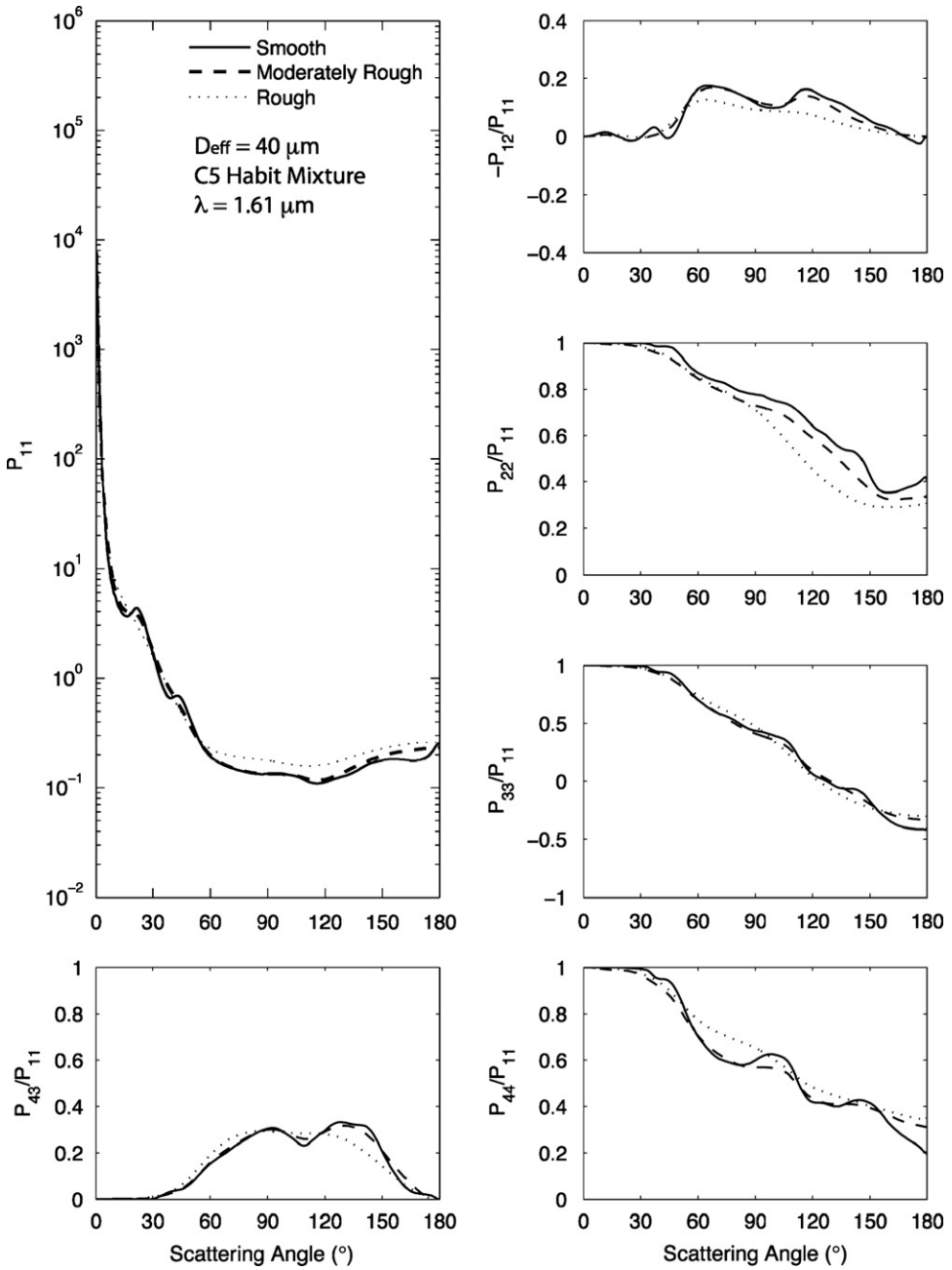

Fig. 8. Same as for Fig. 7 but at a wavelength of 1.61 μm. The values of the asymmetry parameter for smooth, moderately roughened, and severely roughened particles are 0.8258, 0.8176, and 0.7830, respectively.

different dynamical conditions, such as synoptic and tropical anvil cirrus.

4. Phase components obtained from CALIOP data

Over the course of a year, CALIOP data can provide global statistics of P_{11} and P_{22}/P_{11} at Θ=180°, which from the previous analyses is noted to be one of the angles that is most sensitive to crystal habit and surface roughness. P_{11} can be estimated from the layer integrated attenuated backscatter (γ') of ice clouds that are optically thick, defined here as having an optical thickness (τ) greater than 3. P_{11} can also be estimated from γ' for ice clouds that are optically thin when the lidar two-way transmittance of the cloud layer can be estimated from the molecular backscatter below the cloud layer. A full description of the equations governing the interpretation of lidar measurements is provided in [30,31]. The relationship between γ' and the backscatter to extinction ratio, and hence to the normalized scattering phase function at 180°, is

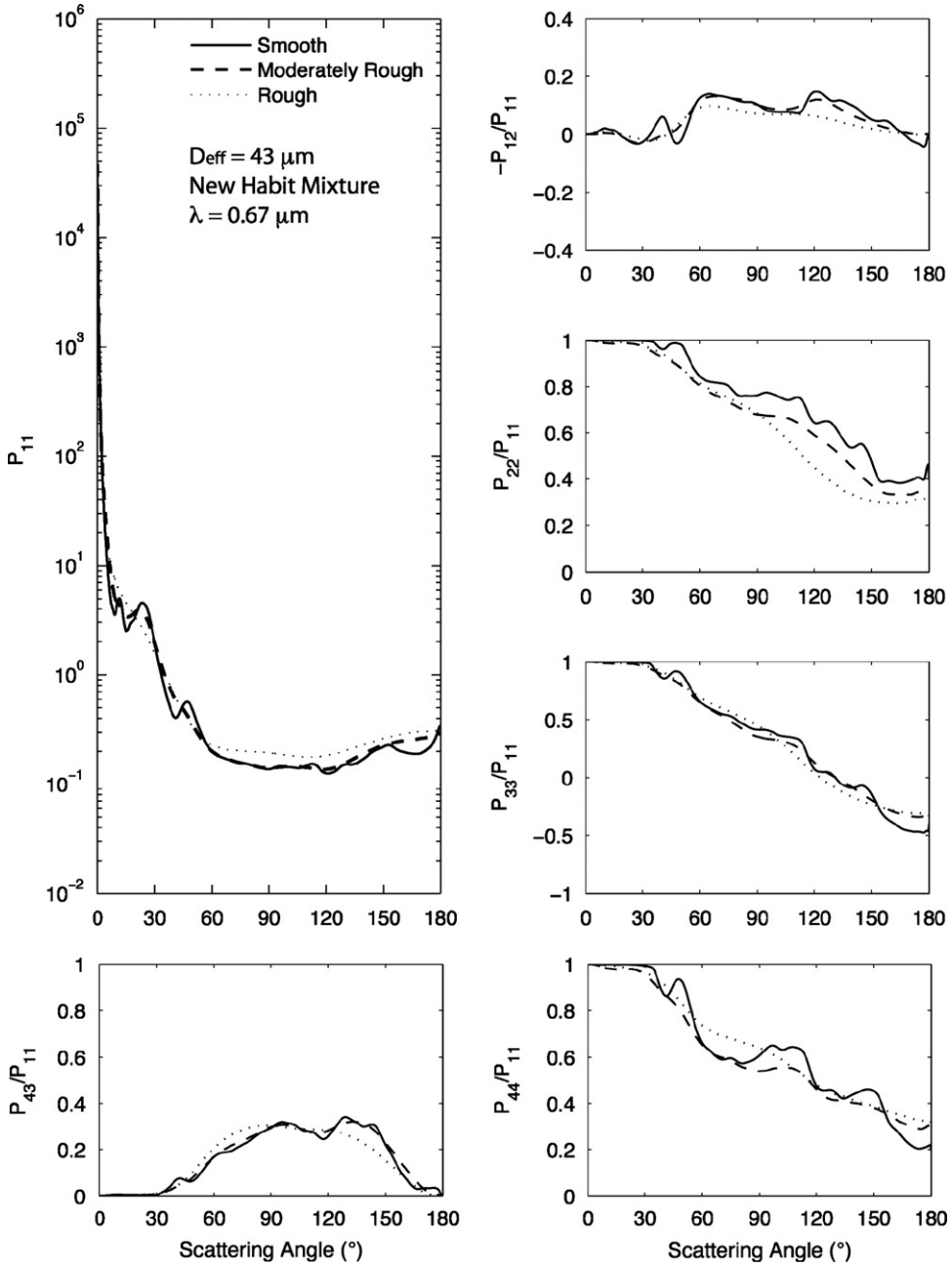

Fig. 9. Phase matrix for the PSD in Fig. 2, using a new habit distribution that includes new habits such as the hollow bullet rosette and aggregate of plates. The wavelength is 0.67 μm and the D_{eff} is 43 μm. The values of the asymmetry parameter for smooth, moderately roughened, and severely roughened particles are 0.8078, 0.8003, and 0.7630, respectively.

given by

$$P_{11} = 2\pi \frac{2\eta\gamma'}{1-\exp(-2\eta\tau)} \approx 2\pi\gamma' \tag{6}$$

assuming that the multiple scattering factor (η) has a value of 0.5 and $\tau > 3$. The linear depolarization ratio δ of lidar backscatter can be estimated from the ratio of the perpendicular backscatter to the parallel backscatter at a given wavelength [32–34]. As discussed in [32], the depolarization ratio associated with a single backscattering event is given by

$$\delta = \frac{P_{11}-P_{22}}{P_{11}+P_{22}}, \tag{7}$$

which can be rearranged to provide P_{22}/P_{11} as follows:

$$\frac{P_{22}}{P_{11}} = \frac{1-\delta}{1+\delta}, \tag{8}$$

CALIOP actually measures the volume depolarization ratio, and this includes the contributions from both molecular and particulate backscatter. For optically thick

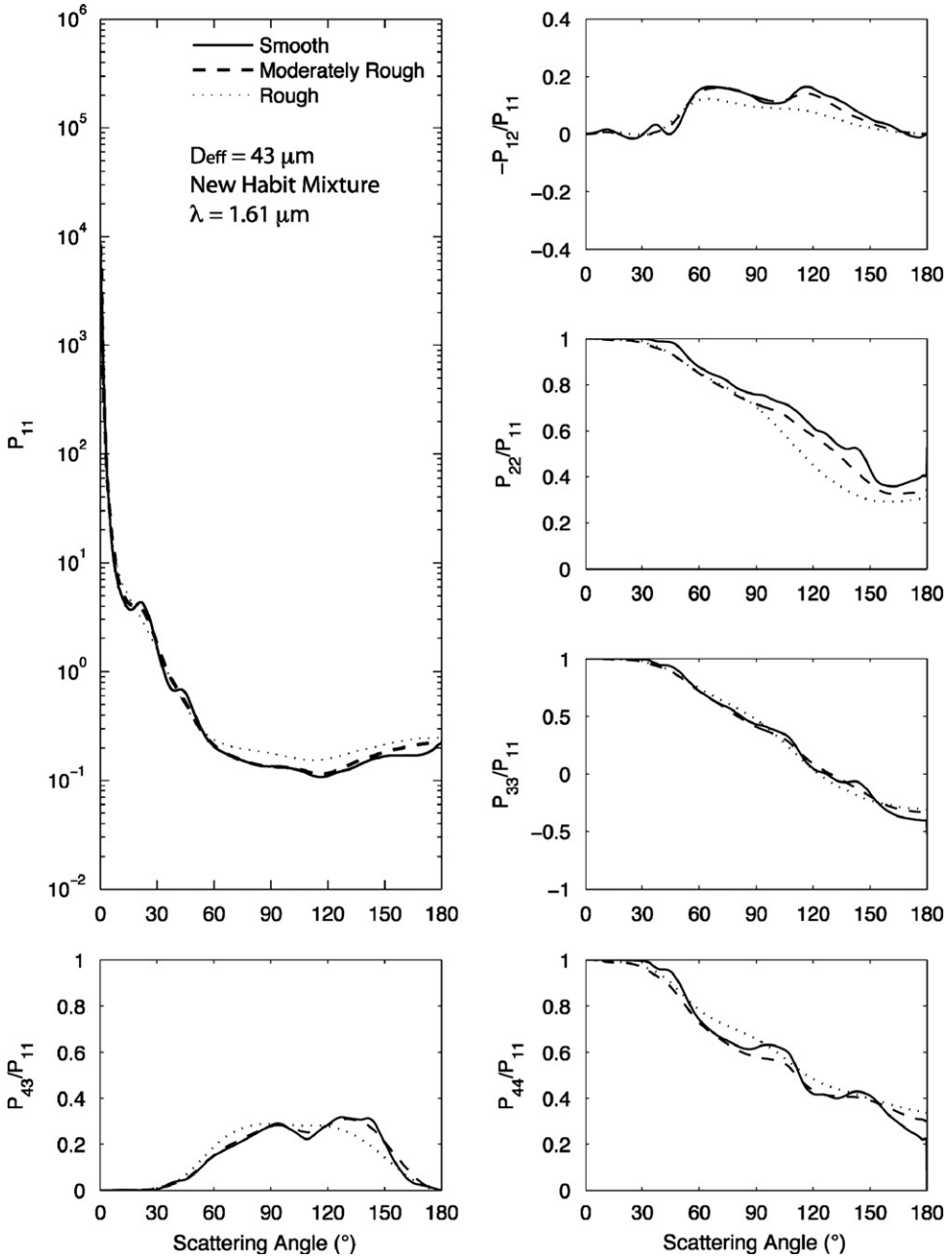

Fig. 10. Phase matrix for the PSD shown in Fig. 2, using the new habit distribution shown in Fig. 1. The wavelength is 1.61 μm and the D_{eff} is 43 μm. The values of the asymmetry parameter for smooth, moderately roughened, and severely roughened particles are 0.8269, 0.8195, and 0.7866, respectively.

ice clouds (extinction coefficient $\gg 0.2\ km^{-1}$), the volume and particulate depolarization ratios are not significantly different from each other. If the molecular backscatter is assumed to be negligible for the 532-nm cross polarization and 1064-nm observations, and if the cloud particulate backscattering is further assumed to be equivalent at both wavelengths, then the cloud particulate depolarization ratio can be estimated as the ratio of the perpendicular backscatter at 532 nm to the parallel backscatter at 1064 nm. The errors in the particulate depolarization ratio can be as high as 0.1 [34].

A full year (2008) of CALIOP layer-integrated cloud backscatter data from the Version 2 5-km Level-2 cloud product was analyzed to study the statistics of P_{11} and P_{22}/P_{11} at $\Theta = 180^{\circ}$. A refined CALIOP cloud phase algorithm [34] is applied to the Level-2 cloud backscatter data for selecting opaque ice cloud layers with randomly oriented particles. This cloud phase approach separates randomly oriented ice particles from those that are horizontally oriented, which is important since the horizontally oriented ice particles have low depolarization and can thus be confused with water clouds. The ice clouds analyzed in this

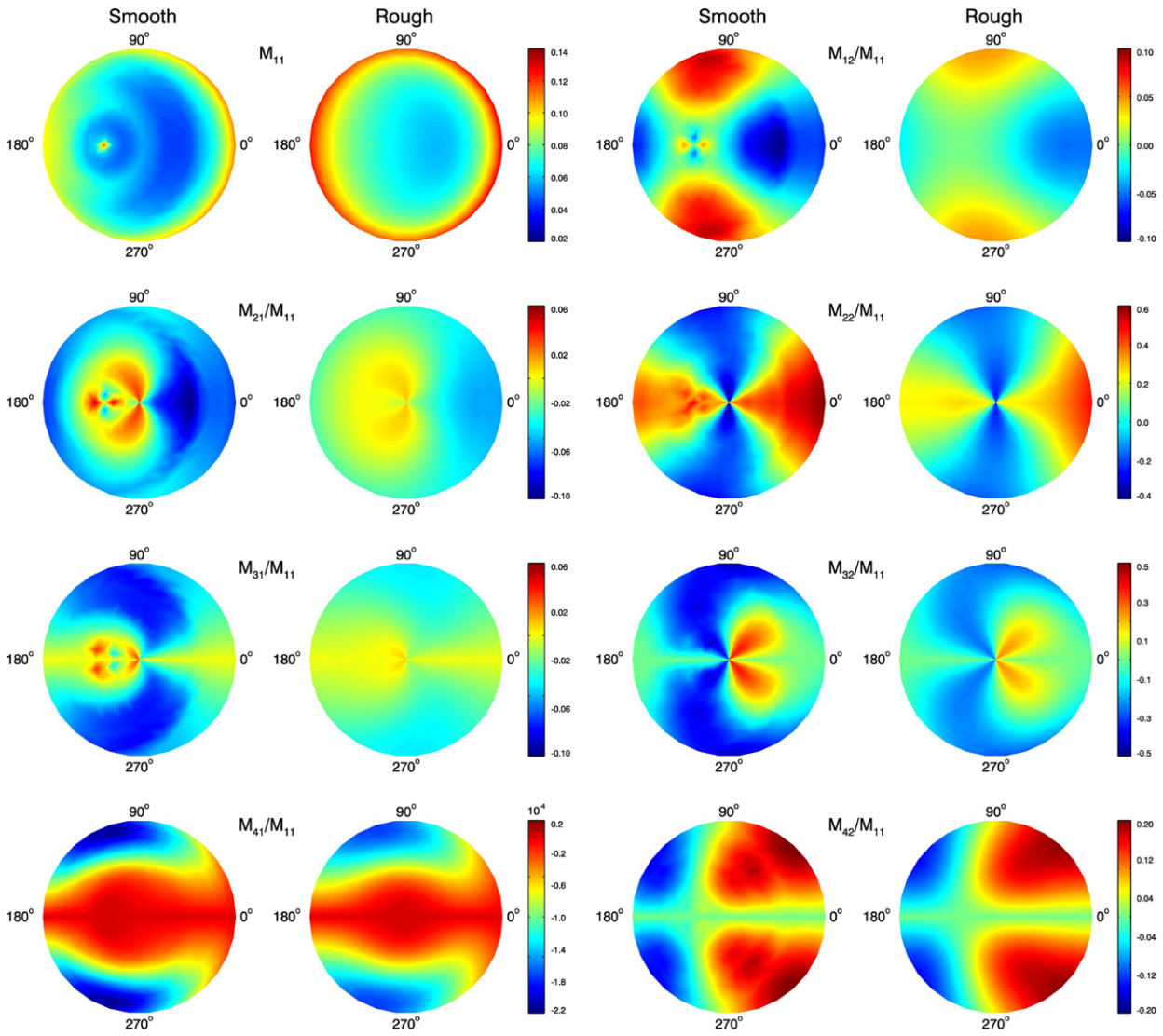

Fig. 11. Comparison of the individual Mueller matrix components for smooth and roughened ice particles using the MODIS C5 habit distribution. Calculations are performed assuming the PSD shown in Fig. 2 at a wavelength of 0.67 μm, a solar zenith angle of 24°, and an ice cloud optical thickness of 1. Note that the values of the M_{22}/M_{11} component at backscattering angles are very sensitive to particle roughening.

study are composed solely of randomly oriented particles with high confidence. Ice clouds that show any sign of horizontal orientation are removed since they may contaminate the P_{11} and P_{22} statistics.

For ice clouds that are both opaque to CALIOP and consisting of randomly oriented particles, Fig. 12 provides the histogram of the temperature dependence of P_{11} and P_{22}/P_{11}. The color represents the frequency of occurrence in logarithmic scale ($\log_{10}$). The cloud temperature in this study is the GEOS-5 air temperature at the mid-layer cloud altitude from the lidar measurement. Fig. 12 shows that the values of P_{11} for most ice clouds range between 0.15 and 0.2 and are relatively insensitive to mid-layer cloud temperature. In contrast, the values of P_{22}/P_{11} range between 0.35 and 0.6 and show a strong correlation with cloud temperature. The depolarization ratios decrease as the cloud temperature increases, and thus P_{22}/P_{11} values for warmer ice clouds are higher than for colder clouds.

The results in Fig. 13 suggest that there is some geographical dependence of the P_{11} and P_{22}/P_{11} values. Mean P_{11} values range between 0.18 and 0.2 for ocean and are slightly higher over land (0.21). At higher latitudes, the mean P_{11} values varies more, ranging between 0.15 and 0.25. Mean P_{22}/P_{11} values range between 0.4 and 0.5. The mean P_{22}/P_{11} values are higher in storm track regions (0.48) then in the lower latitudes (0.42). Histograms of the mean values of P_{11} and P_{22}/P_{11} are provided in Fig. 14.

For comparison with the MODIS C5 habit distribution, the values of P_{11} at $\Theta=180^\circ$ are 0.55 (smooth), 0.24 (moderately rough), and 0.28 (severely roughened). At $\Theta=180^\circ$ the values of P_{22}/P_{11} are 0.4 (smooth), 0.37 (moderately rough), and 0.34 (severely roughened). For the new habit distribution, the values of P_{11} at $\Theta=180^\circ$

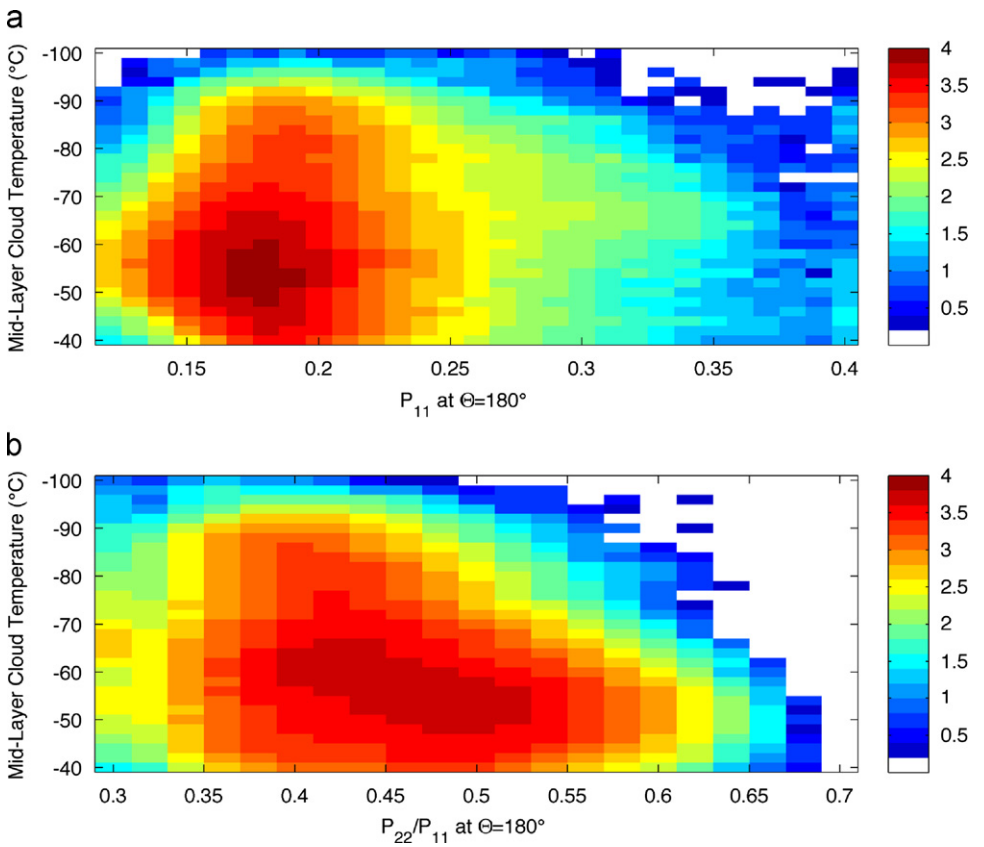

Fig. 12. Based on global CALIOP data from 2008 (Version 2, 5-km product), histograms provide the temperature dependence of (a) P_{11} and (b) P_{22}/P_{11} at the backscattering angle $\Theta=180^{\circ}$. The P_{11} component is derived from the layer-integrated attenuated backscatter. The P_{22}/P_{11} component is derived from the depolarization ratio and provides an indication of particle nonsphericity, where for spherical particles $P_{22}/P_{11}=1$. There seems to be very little dependence of P_{11} on temperature, while P_{22}/P_{11} is strongly temperature dependent. The color is in $\log_{10}$ scale.

are 0.34 (smooth), 0.29 (moderately rough), and 0.33 (severely roughened), and for P_{22}/P_{11} are 0.4 (smooth), 0.34 (moderately rough), and 0.33 (severely roughened). In comparison with the CALIOP analysis, both the C5 and new habit distribution values for P_{11} are higher no matter what roughness is assumed, but the values for P_{22}/P_{11} are lower than those for CALIOP. Further assessment of the assumptions that are used for CALIOP data reduction might shed additional insight as to the differences. Only randomly oriented ice particles are used in the analysis of CALIOP data, and the data are filtered to consider ice clouds at $T_{cld} \leq -40\ ^{\circ}C$. Further investigation is warranted to understand this discrepancy more fully.

5. Summary

This study explores the influence of ice particle habit (or shape) and surface roughness on the scattering phase matrix at two wavelengths: 0.67 and 1.61 μm. For this effort, a database of single-scattering properties has been computed for a set of habits including hexagonal plates, hollow and solid columns, hollow and solid 3D bullet rosettes, droxtals, and aggregates of solid columns. The database provides properties for each of the habits between 0.45 and 2.24 μm for smooth, moderately roughened, and severely roughened particles. One aspect of the single-scattering properties is different from that of previous studies: a new treatment of the forward scattering has been implemented in the scattering calculations that results in the removal of a delta-transmission term at solar wavelengths. At each wavelength, the scattering properties are provided at 233 discrete particle diameters ranging from 2 to 10,000 μm.

In synoptic and convective ice clouds, particles tend to be present over a range of sizes rather than a monodistribution of a single size (with exceptions being jet contrails and wave clouds). A single particle size distribution from a very cold ice cloud sampled during the CRYSTAL-FACE field campaign ($T_{cld}=-76\ ^{\circ}C$) is used to illustrate the influence of habit and roughness on the phase matrix. For a given assumption of particle habits, the single-scattering properties are integrated over the size distribution to provide bulk scattering properties. Droxtals are assumed for the very smallest particles in a size distribution, while solid columns, hollow bullet rosettes, or a habit mixture (following that used in MODIS Collection 5 operational processing) are used for larger particle sizes. Also explored is a new habit distribution that includes the use of three new particles: a hollow bullet rosette, a "small" aggregate of plates (no more than 5 plates, each plate being no larger than 500 μm), and a "large" aggregate of plates (consisting of more than 5

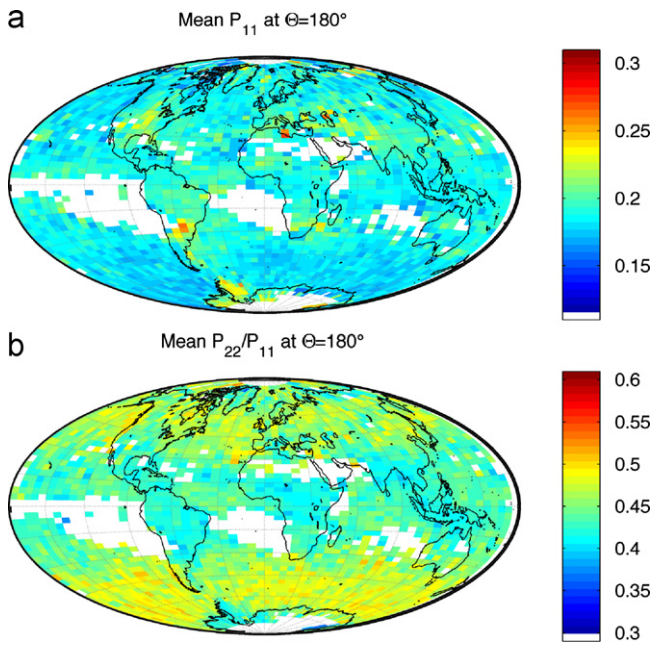

Fig. 13. Global distributions of (a) P_{11} and (b) P_{22}/P_{11} based on a full year of global CALIOP data from 2008 (Version 2, 5-km product). For most of the world, the values of P_{11} range between 0.18 and 0.2. The value of P_{22}/P_{11} may be slightly higher at some locations in the Arctic, but tends to range between 0.4 and 0.5, with values at about 0.48 in the storm tracks.

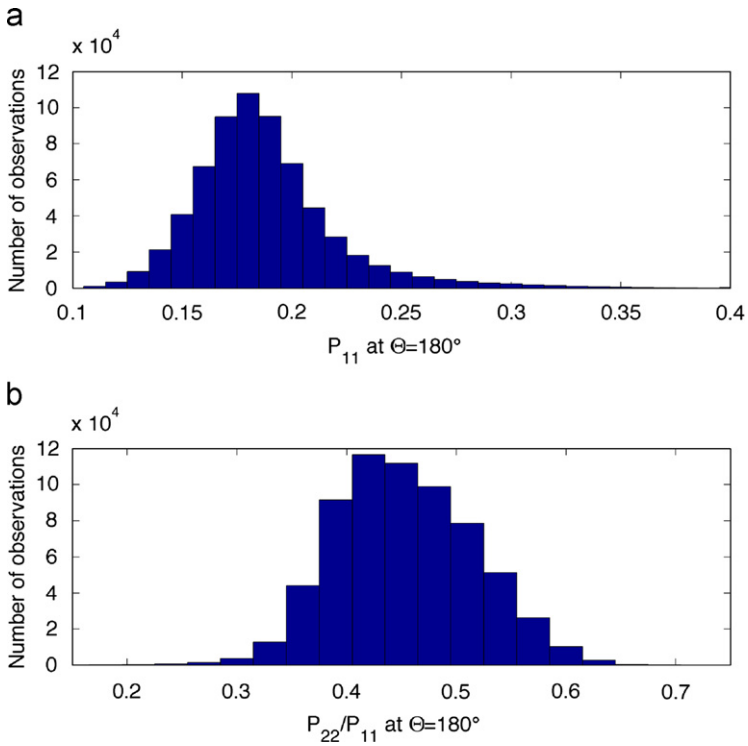

Fig. 14. Histogram of mean values for (a) P_{11} and (b) P_{22}/P_{11} based on a full year of global CALIOP data from 2008 (Version 2, 5-km product).

plates, but each plate can be no larger than 500 μm in maximum dimension).

The full phase matrix is provided for four different habit assumptions at the two wavelengths. All elements of the phase matrix are shown to be quite sensitive to the assumed habit, especially the degree of linear polarization. Surface roughness is shown to smooth out maxima in the scattering phase function and in the other

components of the phase matrix, consistent with other studies.

To compare with the theoretical simulations of the phase matrix for smooth and roughened particles, a full year of CALIOP data from 2008 was analyzed to provide global statistics on the values of P_{11} and P_{22}/P_{11}. In comparison with the CALIOP analysis, the P_{11} values for both the C5 and new habit distributions are higher no matter what particle surface roughness is assumed, while the values for P_{22}/P_{11} are slightly lower than those for CALIOP.

While important information provided by the depolarization lidar, another critical piece of information can be provided by space-based polarimetric data, which can measure the $-P_{21}/P_{11}$ component of the phase matrix. Such polarimetric data have been available from POLDER. While data from POLDER will be the topic of further study using the scattering properties discussed in this study, the advent of multi-angle, multi-wavelength polarimetric data from a sensor like GLORY [35] will be even more valuable for determining how much roughness to assume for global analyses of ice clouds, for example.

Acknowledgments

Drs. Baum and Yang gratefully acknowledge the funding of this work through a NASA grant (NNX08AF81G), and note the support and encouragement of Dr. Hal Maring at NASA headquarters. Dr. Yang's research is also partly supported by another NASA grant (NNX08AI94G) supervised by Dr. Charles Trepte as the technical officer.

References

[1] Baum BA, Heymsfield AJ, Yang P, Bedka ST. Bulk scattering models for the remote sensing of ice clouds. Part 1: Microphysical data and models. J Appl Meteor 2005;44:1885–95.
[2] Baum BA, Yang P, Heymsfield AJ, Platnick S, King MD, Bedka ST. Bulk scattering models for the remote sensing of ice clouds. Part 2: Narrowband models. J Appl Meteor 2005;44:1896–911.
[3] Kokhanovsky A, Macke A. The dependence of the radiative characteristics of optically thick media on the shape of particles. JQSRT 1997;63:393–407.
[4] Van Diedenhoven B, Hasekamp OP, Landgraf J. Retrieval of cloud parameters from satellite-based reflectance measurements in the ultraviolet and the oxygen A-band. J Geophys Res 2007;112: D15208, doi:10.1029/2006JD008155.
[5] Platnick S, King MD, Ackerman SA, Menzel WP, Baum BA, Riedl C, et al. The MODIS cloud products. algorithms and examples from Terra. IEEE Trans Geosci Remote Sens 2003;41:459–73.
[6] Yang P, Zhang L, Hong G, Nasiri SL, Baum BA, Huang HL, et al. Differences between collection 4 and 5 MODIS ice cloud optical/microphysical products and their impact on radiative forcing simulations. IEEE Trans Geosci Remote Sens 2007;45:2886–99.
[7] Zhang Z, Yang P, Kattawar GW, Riedi J, Labonnote LC, Baum BA, et al. Influence of ice particle model on satellite ice cloud retrieval: lessons learned from MODIS and POLDER cloud product comparison. Atmos Chem Phys Discuss 2009;9:1757–96.
[8] Born M, Wolf E. In: Principles of optics. 4th edition. Oxford, London: Pergamon Press; 1970 pp. 808.
[9] Baran AJ, Labonotte LC. On the reflection and polarisation properties of ice cloud. JQSRT 2006;100:41–54.
[10] Nousiainen T, Muinonen K. Surface-roughness effects on single-scattering properties of wavelength-scale particles. JQSRT 2007;106:389–97.
[11] Shcherbakov V, Gayet JF, Jourdan O, Strom J, Minikin A. Light scattering by single ice crystals of cirrus clouds. Geophys Res Lett 2006:L15809, doi:10.1029/2006GL026055.
[12] Ulanowski Z, Hesse E, Kaye PH, Baran AJ. Light scattering by complex ice-analogue crystals. JQSRT 2006;100:382–92.
[13] Chepfer H, Brogniez G, Goloub P, Breon FM, Flamant PH. Observations of horizontally oriented ice crystals in cirrus clouds with POLDER-1/ADEOS-1. JQSRT 1999;63:521–43.
[14] Chepfer H, Goloup P, Reidi J, De Haan J, Hovenier J, Flamant PH. Ice crystal shapes in cirrus clouds derived from POLDER-1/ADEOS-1. J Geophys Res 2001;106:7955–66.
[15] Riedi J, Doutriaux-Boucher M, Goloub P, Couvert P. Global distribution of cloud top phase from POLDER/ADEOS1. Geophys Res Lett 2000;27:1707–10.
[16] Noel V, Chepfer H. Study of ice crystal orientation in cirrus clouds based on satellite polarized radiance measurements. J Atmos Sci 2004;61:2073–81.
[17] Labonnote LC, Brogniez G, Buriez JC, Doutriaux-Boucher M, Gayet JF, Macke A. Polarized light scattering by inhomogeneous hexagonal monocrystals. Validation with ADEOS-POLDER measurements. J Geophys Res 2001;106:12139–53.
[18] Yang P, Liou KN, Wyser K, Mitchel D. Parameterization of the scattering and absorption properties of individual ice crystals. J Geophys Res 2000;105:4699–718.
[19] Yang P, Baum BA, Heymsfield AJ, Hu YX, Huang HL, Tsay SC, et al. Single scattering properties of droxtals. JQSRT 2003;79-80: 1159–69.
[20] Yang P, Zhang Z, Kattawar GW, Warren SG, Baum BA, Huang HL, et al. Effect of cavities on the optical properties of bullet rosettes: implications for active and passive remove sensing of ice cloud properties. J Appl Meteor Clim 2008;47:2311–30.
[21] Bi L, Yang P, Kattawar GW, Baum BA, Hu YX, Lu JQ. Simulation of the color ratio associated with the backscattering of radiation by ice crystals at 0.532 and 1.064-μm wavelengths. J Geophys Res 2009;114(D00H08)10.1029/2009JD011759.
[22] Yang P, Kattawar GW, Hong G, Minnis P, Hu YX. Uncertainties associated with the surface texture of ice particles in satellite-based retrieval of cirrus clouds: Part I. Single-scattering properties of ice crystals with surface roughness. IEEE Trans Geosci Remote Sens 2008;46:1940–7.
[23] Warren SG, Brandt RE. Optical constants of ice from the ultraviolet to the microwave: a revised compilation. J Geophys Res 2008;113:D14220, doi:10.1029/2007JD009744.
[24] de Haan JF, Bosma PB, Hovenier JW. The adding method for multiple scattering calculations of polarized light. Astron Astrophys 1987;183:371–91.
[25] Kattawar GW, Rakovic MJ. Virtues of Mueller matrix imaging for underwater target detection. Appl Opt 1999;38:6431–8.
[26] Yang P, Wei HL, Kattawar GW, Hu YX, Winker DM, Hostetler CA, et al. Sensitivity of the backscattering Mueller matrix to particle shape and thermodynamic phase. Appl Opt 2003;42:4389–95.
[27] Mishchenko MI, Travis LD. Satellite retrieval of aerosol properties over the ocean using polarization as well as intensity of reflected sunlight. J Geophys Res 1997;102:16989–7013.
[28] Heymsfield AJ, Bansemer A, Field PR, Durden SL, Stith J, Dye JE, et al. Observations and parameterizations of particle size distributions in deep tropical cirrus and stratiform precipitating clouds: results from in situ observations in TRMM field campaigns. J Atmos Sci 2002;59: 3457–91.
[29] Mishchenko MI, Travis LD, Lacis AA. In: Scattering, absorption and emission of light by small particles. Cambridge, UK: Cambridge University Press; 2002 445 pp.
[30] Platt CMR. Remote sounding of high clouds: I. Calculation of visible and infrared optical properties from lidar and radiometer measurements. J Appl Meteor 1979;18:1130–43.
[31] Platt CMR, Dilley AC. Remote sounding of high clouds. IV: observed temperature variations in cirrus optical properties. J Atmos Sci 1981;38:1069–82.
[32] Hu YX, Vaughan M, Liu ZY, Lin B, Yang P, Flittner D, et al. The depolarization-attenuated backscatter relation: CALIPSO lidar measurements vs. theory. Opt Express 2007;15:5327–32.
[33] Hu XY. Depolarization ratio-effective lidar ratio relation: theoretical basis for space lidar cloud phase discrimination. Geophys Res Lett 2007;34:L11812, doi:10.1029/2007GL029584.
[34] Hu XY, Winker D, Vaughan M, Lin B, Omar A, Trepte C, et al. CALIPSO/CALIOP cloud phase discrimination algorithm. J Atmos Oceanic Tech 2009;26:2293–309.
[35] Mishchenko MI, Cairns B, Kopp G, Schueler CF, Fafaul BA, Hansen JE, et al. Accurate monitoring of terrestrial aerosols and total solar irradiance: introducing the Glory mission. Bull Am Meteorol Soc 2007;88:677–91.